Supporting Information

R. Gregor Weiß,[1,2] Matthias Heyden,[3] and Joachim Dzubiella[1,2,*]

[1] *Department of Physics, Humboldt Universität zu Berlin, Newtonstr. 15, D-12489 Berlin, Germany, Germany*

[2] *Soft Matter and Functional Materials, Helmholtz-Center Berlin, Hahn-Meitner Platz 1, D-14109 Berlin, Germany*

[3] *Max-Planck-Insitut für Kohlenforschung, Kaiser-Wilhelm-Platz 1, D-45470 Mülheim an der Ruhr, Germany*

Molecular Dynamics Simulations

The systems comprise SPC/E water as solvent and a single hydrophobic sphere fixed in the middle of the simulation box. The interaction between SPC/E and the model solute is mediated by a shifted Lennard Jones potential $U_{LJ}(r') = 4\epsilon[(\sigma/r')^{12} - (\sigma/r')^6]$ whereas $r' = r - r_0$ increases the solute size. The parameters $\epsilon = 1.197\,\mathrm{kJ/mol}$ and $\sigma = 3.768\,\text{Å}$ are those of a united-atom methane molecule as in Ref.[1]. Ten seperate simulations are performed with shift radii $r_0 = 0\,\text{Å}$, $1\,\text{Å}$, $2\,\text{Å}$, $4\,\text{Å}$, $6\,\text{Å}$, $8\,\text{Å}$, $10\,\text{Å}$, $12.5\,\text{Å}$, $15\,\text{Å}$ and $17.5\,\text{Å}$. For shift radii $r_0 \leq 6\,\text{Å}$ the simulation box containes 6000 SPC/E water molecules and for simulations with $r_0 > 6\,\text{Å}$ the number of solute molecules is doubled to 12000 to avoid finite size effects.

To model the corresponding hydrophobic surface without curvature the walls in the x-y-plane of a simulation box of size $5.67 \times 5.67 \times 6.54\,\mathrm{nm}^3$ are set to interact with water with a 12-6 potential in the z-direction $U_{12-6}(z) = 4\epsilon[(\sigma/z)^{12} - (\sigma/z)^6]$ with same interaction parameters $\epsilon = 1.197\,\mathrm{kJ/mol}$ and $\sigma = 3.768\,\text{Å}$.

Each system is equilibrated in NPT ensemble for 100 ps at ambient conditions, namely $T = 300\,\mathrm{K}$ and $P = 1\,\mathrm{bar}$. After equilibration the box lengths of the cubic boxes are roughly 5.65 nm and 7.15 nm for the small (6000 SPC/E) and big (12000 SPC/E) setups respectively. In order to gather enough statistics to probe long-time dynamics within the thin solvation shell comprised of $\mathcal{O}(10)$ to $\mathcal{O}(10^2)$ water molecules subsequent production runs have a length of 200 ns for the small systems and 100 ns for the big systems with a time step of 2 fs and writing period of 200 fs. Energy divergence is prevented by simulation in NVT ensemble ($T = 300\,\mathrm{K}$) applying the Nosé-Hoover thermostat with a coupling period of 1 ps. The Nosé-Hoover is implemented by an extra degree of freedom introduced as a heat bath within the hamiltionian of the simulation and thus has the advantage of creating physically more realistic NVT ensembles [5, 6].

Additional simulations for the cavities with $r_0 = 0\,\text{Å}$, $1\,\text{Å}$, $2\,\text{Å}$ and $4\,\text{Å}$ were performed in order to resolve the temperature dependence of our observations. Production runs with $T = 260\,\mathrm{K}$, $280\,\mathrm{K}$ and $320\,\mathrm{K}$ were performed up to 100 ns.

All simulations are performed with the GROMACS 4.5.4 package [4].

Planar Limit

The spatial distribution function in figure 1 of water at planar walls with the interaction parameters mentioned above does not exhbit a clear first and second minimum. The missing extrema hinder a clear definition of a first and second solvation shell as it can be observed from the RDFs (main text Fig. 1) for curved surfaces.

One further simulation of a wall interacting with a doubled interaction strength $\epsilon = 2.394\,\mathrm{kJ/mol}$ was conducted to generate clear extrema (Fig. 1) and hence definitions for the solvation layers. Clearly, the found borders to the solvation shells only approximate values that correspond to values that would consistently define hydration layers for the original interaction parameters.

Another notable difference to simulations of water at curved surfaces arrises from the lack of long-range correction for the interaction in the planar geometry. This creates smaller water densities and larger mobilities than in bulk [3].

Both discrepancies introduce minor consistency deviations between the simulations with the curved surfaces and the planar limit but never conflict with our interpretation.

MFPT method and perpendicular diffusivity

In the main text we briefly describe the MFPT method from Hinczewski *et al.* [2] which takes the free energy profile $F(r)$ and the spatial derivative of the MFPT curve $T_{fp}(r, r_t)$. Both are obtained equivalently to the application of

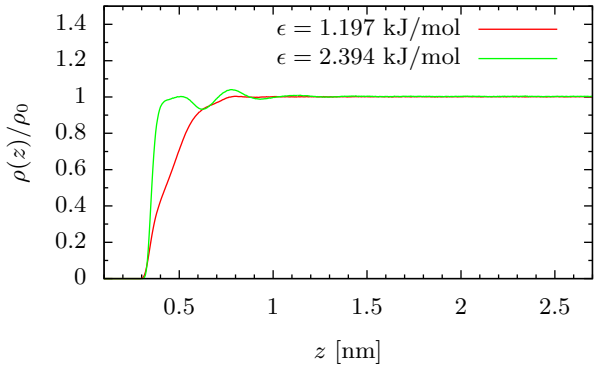

Fig. 1: Normalized water distribution at hydrophobic walls.

pair diffusion of water and methane by Sedlmeier *et al.* [3]. The integral $\int_{r_{min}}^{r} \mathrm{d}r\, \mathrm{e}^{-\beta F(r)}$ is evaluated numerically starting from the reflective boundary r_{min}, which we define by the largest distance from the respective solute where $F(r_{min}) \geq 10\ k_B\mathrm{T}$. The derivative $\partial\, T_{fp}(r, r_t)/\partial r$ is determined by fitting a linear function to the function values around $r - \delta r < r < r + \delta r$ whereas $\delta r = 0.05$ nm. The closest distance r evaluated for the derivative, and hence diffusivity profile value closest to the solute, is $r \lessapprox R_G$ where statistics of $T_{fp}(r, r_t)$ allow a reasonable fit in the mentioned range of δr.

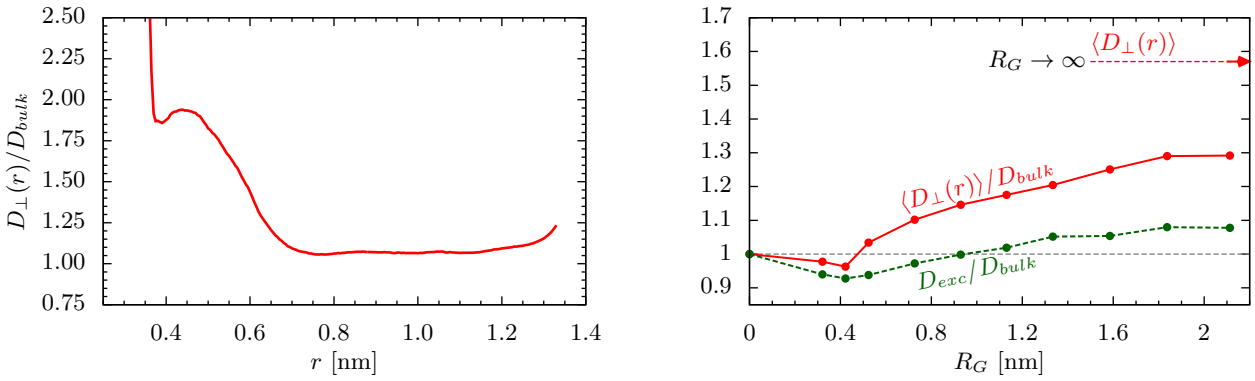

Fig. 2: Left panel: Spatially resolved perpendicular diffusion profile of water at the hydrophobic wall. Right panel: (red, solid) Average perpendicualr diffusion constant $\langle D_\perp(r)\rangle$ (eq. 1) inside the solvation layer of differently sized hydrophobic model solutes. The red horizontally dashed line is the corresponding value at the planar limit ($R_G \to \infty$) for $\langle D_\perp(r)\rangle$ (green, dashed) Excess perpendicular diffusion constant $D_{exc} + 1$ (eq. 2) quantifying an average disruption of the diffusion of water near hydrophobic solutes. The reference value of bulk diffusivity is drawn as grey horizontally dashed line as isoline with value 1.

The left panel of Fig.2 plots the diffusivity profile of water motion perpendicular to the hydrophobic planar model surface. The diffusivity right at the surface decreases rapidly from high mobility values to a global minimum proceeding into a maximum which is located within the hydration water layer. With growing distance to the wall the diffusivity then decreases to bulk diffusion. The minimum at the outer margin of the solvation shell which is visible in each profile in Fig.4 of the main text almost fully vanishes for the profile of the planar surface here.

The right panel in Fig.2 shows two further measures quantifying the perpendicular diffusivity in vicinity of the hydrophobic model solutes. The red curve is an average diffusivity inside the first solvation shell

$$\langle D_\perp(r)\rangle = \int_{R_{max}}^{R_1} \mathrm{d}r\, g_{so}(r) \cdot D_\perp(r) \quad . \tag{1}$$

It captures the non-monotonicity from the diffusivity profiles slightly decreasing below bulk diffusion near small solutes and subsequently increases converging towards the value for perpendicular diffusion at the planar interface.

We also calculate an "excess" perpendicular diffusivity D_{exc} which quantifies an average change of the diffusivity

constant in the solute's surrounding water

$$D_{exc} = \int_{R_{max}}^{\infty} \mathrm{d}r\, r^2 g_{so}(r) \cdot [D_{\perp}(r)/D_{bulk} - 1] \quad . \tag{2}$$

The plot shows $1+D_{exc}(R_G)$. Certainly the non-monotonic curvature dependence in the diffusivity profiles is smoothly captured in this quantity aswell. In general an excess diffusivity constant can be of particular interest in order to estimate water diffusivity changes in dilute solutions of hydrophobic solutes.

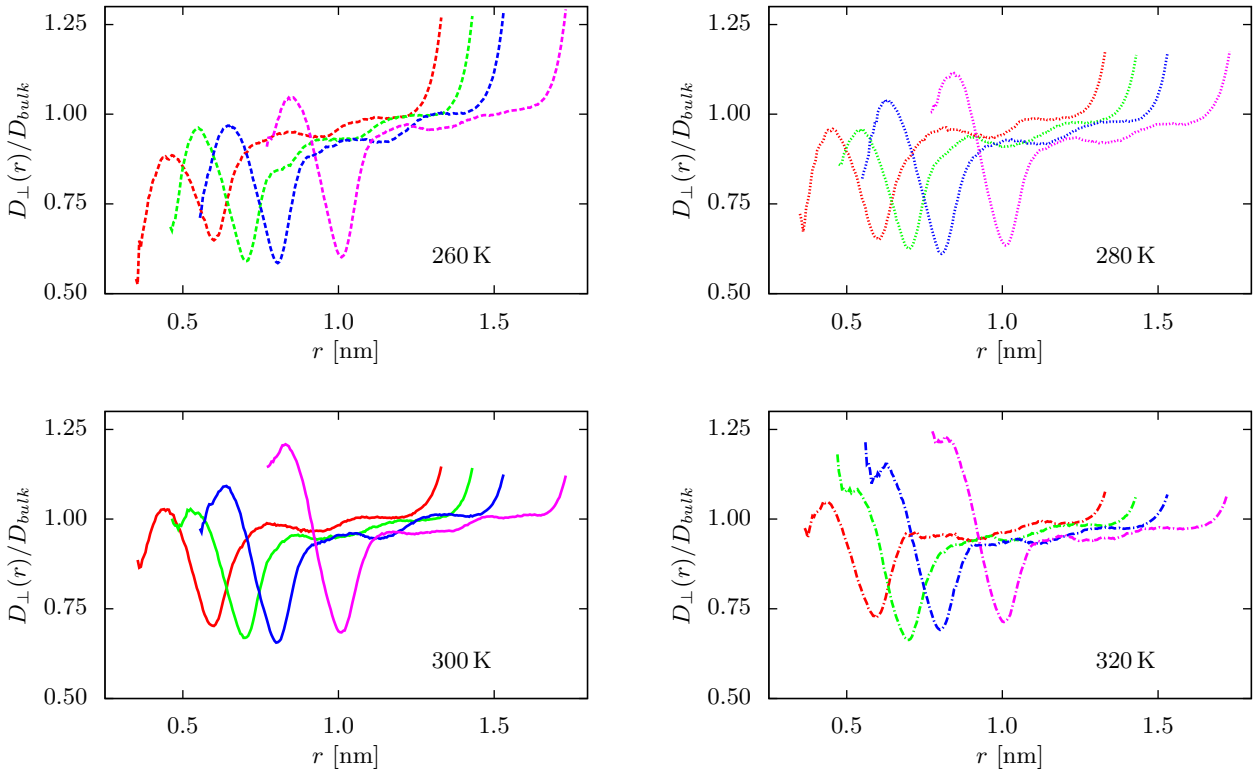

Fig. 3: Perpendicular diffusion at cavities with $r_0 = 0$ Å, 1 Å, 2 Å and 4 Å with temperatures $T = 260$ K (upper left), $T = 280$ K (upper right), $T = 300$ K (bottom left) and $T = 320$ K (bottom right).

Hydrogen Bond Time Correlation

We analyse the autocorrelation function $c(t)$ of the H-bond existence inside the first hydration layer using an in-house analysis code. It uses a geometric H-bond definition with a minimum donor-acceptor distance $d_{HB} \leq 3.5$ Å and donor-hydrogen-acceptor angle $\theta_{HB} \geq 150°$.

Fig. 4 plots the correlation functions $c(t)$ for hydrogen bonds inside the first hydration layer. Hydrogen bonds were selected at time 0 if they were intact and both, acceptor and donor molecules, resided in the first hydration shell. We evaluate $c(t)$ up to correlation times of 100 ps until when it has decayed to magnitudes of 10^{-3}. Therefore, the integral over the correlation function in this time window provides a reasonable lower boundary to the actual HB lifetimes.

In addition the average number of hydrogen bonds per water molecule n within the solvation layer was counted and presented in the main text. The error of the average number of hydrogen bonds per molecule is estimated by block averaging. Using a frequency of a 1000 ps the average number of hydrogen bonds within a block of 100 ps length was calculated, giving 100 uncorrelated block averages n_{Block}. These were used to approximate the standard deviation error by $\delta n = [\Sigma_{Blocks}\,(n - n_{Block})^2/100]^{1/2}$.

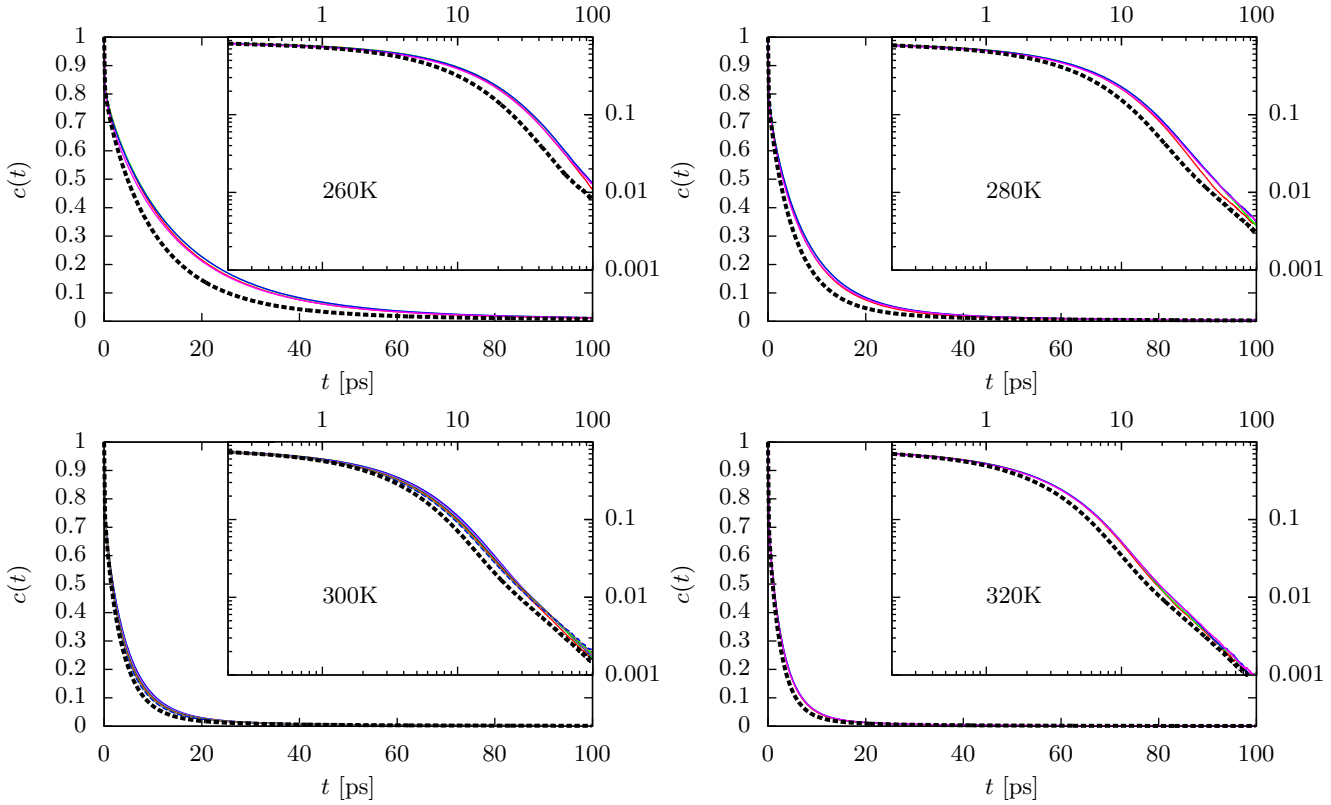

Fig. 4: Correlation function $c(t)$ of the hydrogen bonding operator $h(t)$ of hydrogen bonds on water molecules inside the first solvation shell with temperatures $T = 260\,\mathrm{K}$ (upper left), $T = 280\,\mathrm{K}$ (upper right), $T = 300\,\mathrm{K}$ (bottom left) and $T = 320\,\mathrm{K}$ (bottom right). Only at $T = 300\,\mathrm{K}$ all cavity sizes were evalutated. For the rest the analysis was limited to cavities with $r_0 = 0\,\text{Å}$, $1\,\text{Å}$, $2\,\text{Å}$ and $4\,\text{Å}$.

Temperature dependence of hydrogen bond dynamics

The hydrogen bond correlation function $c(t)$ contains all three time scales of the reaction-diffusion model from Luzar and Chandler [7] given by

$$\begin{aligned}\frac{\partial}{\partial t}\rho(\vec{r},t) &= D\nabla^2\rho(\vec{r},t) + \delta(\vec{r})\,\bar{k}c(t) - \delta(\vec{r})\,\bar{k}'n(t)\\ &\equiv D\nabla^2\rho(\vec{r},t) + k(t)\delta\vec{r},\end{aligned}$$

where the rates $\bar{k}$ and $\bar{k}'$ are those for breaking and reformation of a hydrogen bond, respectively. $n(t)$ is proportional to the diffusivity since $n(t) \propto \rho(0,t)$ [8] (and $\rho(r,t)$ obeying Fick's law).

Thus, as we used the reactive flux $k(t) = -\dot{c}(t)$ to evaluate the *zero frequency part*

$$\tau = \int c(t)\,\mathrm{d}t = \int \frac{k(t) + \bar{k}'n(t)}{\bar{k}}\,\mathrm{d}t\,,$$

the correlation time τ contains the factor $D\bar{k}'/\bar{k}$, which precludes a direct one-to-one connection to the temperature dependence of the diffusivity. Certainly a direct relation of temperature dependence between hydrogen bond dynamics and diffusivity is restored if the time scales were extracted separately.

* To whom correspondence should be addressed. E-mail: joachim.dzubiella@helmholtz-berlin.de

[1] D. M. Huang and D. Chandler J. Phys. Chem. B **106** 2047-2053 (2002)
[2] M. Hinczewski, Y. von Hansen, J. Dzubiella and R. R. Netz J. Chem. Phys. **132** 245103 (2010)

[3] F. Sedlmeier, Y. von Hansen, L.Mengyu, D. Horinek and R. R. Netz J. Stat. Phys. **145** 240-252 (2011)
[4] B. Hess, C. Kutzner, D. van der Spoel, and E. Lindahl J. Chem. Theory Comput. **4** 435 (2008)
[5] S. Nosé J. Chem. Phys. **81** 511 (1984)
[6] W. G. Hoover Physical Review A **31** 1695 (1985)
[7] A. Luzar and D. Chandler Nature **437** 640-647 (1996)
[8] A. Luzar J. Chem. Phys. **113** 23 (2000)